

Approximate Symmetries in Nuclear Structure

Dennis Bonatsos

Institute of Nuclear Physics, N.C.S.R. “Demokritos”, GR-15310 Aghia Paraskevi, Attiki, Greece

Abstract. Dynamical symmetries have played a central role for many years in the study of nuclear structure. Recently, the concepts of Partial Dynamical Symmetry (PDS) and Quasi-Dynamical Symmetry (QDS) have been introduced. We shall discuss examples of PDS appearing in the framework of geometrical collective models, as well as examples of PDS and QDS appearing in the large boson number limit of the Interacting Boson Model.

1 Introduction

Dynamical symmetries have been used in nuclear structure for several years. A well known example is provided by the Interacting Boson Model [1], having an overall $U(6)$ symmetry, within which the dynamical symmetries $U(5)$ [corresponding to vibrational nuclei], $SU(3)$ [representing prolate axially deformed nuclei], and $O(6)$ [describing nuclei soft with respect to axial asymmetry (γ -soft)] occur. These dynamical symmetries are traditionally placed at the corners of the symmetry triangle of IBM [2], depicted in Figure 4.

More recently, two new kinds of symmetries have been considered, the Partial Dynamical Symmetries (PDS) [3–6] and the Quasi-Dynamical Symmetries (QDS) [7–11].

There are three kinds of Partial Dynamical Symmetries [3–6]:

- (i) Type I, where some of the states preserve all the relevant symmetry;
- ii) Type II, in which all the states preserve part of the dynamical symmetry;
- iii) Type III, where some of the states preserve part of the dynamical symmetry.

In Section 2 we will show [12, 13] that a PDS of Type I characterizes the 0^+ states of several special solutions of the Bohr Hamiltonian. Furthermore, in Section 3 we will show [14] that signs of a yet unknown PDS seem to appear near the critical line [15–17] of the IBM.

On the other hand, Quasi-Dynamical Symmetries [7–11] are defined as the situations in which dynamical symmetries persist despite strong symmetry-breaking interactions. In Section 4 we will show [18] that such a QDS appears to be providing an explanation for the existence of the Alhassid–Whelan arc of regularity [19, 20] among chaotic regions within the symmetry triangle of the IBM.

2 Partial Dynamical Symmetry for 0^+ states of special solutions of the Bohr Hamiltonian

Several special solutions of the Bohr Hamiltonian have been developed in relation to critical point symmetries, appearing in regions of the nuclear chart where abrupt changes from one nuclear shape to another are observed [21, 22]. In particular, the E(5) critical point symmetry [23] corresponds to the second order shape/phase transition between spherical and γ -unstable nuclei, while the X(5) solution [24] corresponds to the first order shape/phase transition between spherical and prolate axially deformed nuclei. In both cases the Bohr Hamiltonian in 5 dimensions is used. Fixing $\gamma = 0$ in the later case, one obtains X(3) [25], a solution of the Bohr Hamiltonian in 3 dimensions. Z(5) [26] is a solution for $\gamma \approx 30^\circ$, related to triaxial nuclei, while Z(4) [27] is a similar solution in 4 dimensions with γ fixed to 30° .

In these special solutions, an infinite square well potential is used in the β degree of freedom, the solutions being Bessel functions J_ν . The order ν for several different models is shown in Table 1. One can easily see that in all models of this kind the energies of the 0^+ states are given by [12, 13]

$$E(0_m^+) = An \left(n + \frac{D+1}{2} \right), \quad n = m - 1 \quad (1)$$

where D is the number of degrees of freedom in the given model.

The consequences of this result can be seen in Figure 1. While the 0^+ states in the various models appear different when normalized to the first excited 2^+ state, they become identical if they are normalized to the first excited 0^+ state. It is worth remarking in Figure 1 that, surprisingly, the same behaviour appears

Table 1. Order ν , dimension, D , of the model space and ν for $J^\pi = 0^+$ states in the geometrical models E(5), X(5), Z(5), Z(4), and X(3). J is the spin of the level, $\tau = J/2$ (in the ground state band), and n_w is the wobbling quantum number [28], which is zero for 0^+ states. Taken from Ref. [13].

Model	ν	D	$\nu(J=0^+)$
E(5)	$\tau + \frac{3}{2}$	5	$\frac{3}{2}$
X(5)	$\sqrt{\frac{J(J+1)}{3} + \frac{9}{4}}$	5	$\frac{3}{2}$
Z(5)	$\frac{\sqrt{J(J+4) + 3n_w(2J - n_w) + 9}}{2}$	5	$\frac{3}{2}$
Z(4)	$\frac{\sqrt{J(J+4) + 3n_w(2J - n_w) + 4}}{2}$	4	1
X(3)	$\sqrt{\frac{J(J+1)}{3} + \frac{1}{4}}$	3	$\frac{1}{2}$

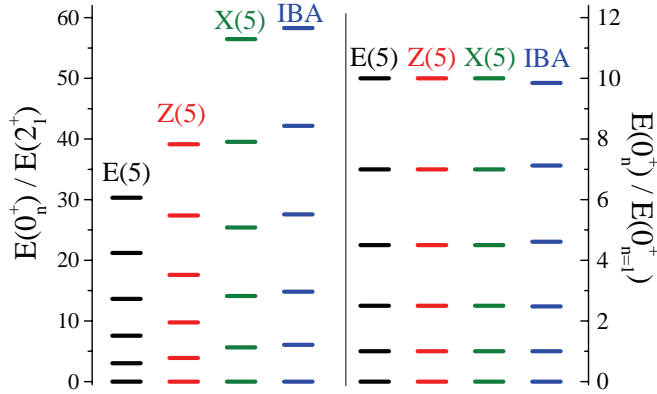


Figure 1. (Left) Energies of excited 0^+ states in the E(5), Z(5), and X(5) models as well as an IBA calculation near the critical point (see text). (Right) Same as left with the energies normalized to the first excited 0^+ state energy. Taken from Ref. [12].

approximately near the critical region of the IBM. We shall further refer to this fact in Section 3.

Considering the properties of the 0^+ states within the Euclidean algebras E(D), one can prove [13] that in all cases the 0^+ states of the models given in Table 1 fulfill the corresponding E(D) symmetry. We thus have a PDS of Type I, in which some of the states (the 0^+ states) preserve all the symmetry, which is the E(D) symmetry in this case.

3 Signs of PDS near the critical region of the IBM

We now focus attention on the IBM, especially at large boson numbers. We use an IBA Hamiltonian of the form [29]

$$H(\zeta, \chi) = c \left[(1 - \zeta) \hat{n}_d - \frac{\zeta}{4N_B} \hat{Q}^x \cdot \hat{Q}^x \right], \quad (2)$$

where $\hat{n}_d = d^\dagger \cdot \tilde{d}$, $\hat{Q}^x = (s^\dagger \tilde{d} + d^\dagger s) + \chi (d^\dagger \tilde{d})^{(2)}$, N_B is the number of valence bosons, and c is a scaling factor. The above Hamiltonian contains two parameters, ζ and χ , with the parameter ζ ranging from 0 to 1, and the parameter χ ranging from 0 to $-\sqrt{7}/2$. The U(5) symmetry is given by $\zeta = 0$, any χ , the SU(3) symmetry by $\zeta = 1$ and $\chi = -\sqrt{7}/2$, and the O(6) symmetry by $\zeta = 1$ and $\chi = 0$. With this parameterization, the entire symmetry triangle, shown in Figure 4, can be described, along with each of the three dynamical symmetry limits. Calculations in this work have been performed with the code IBAR [30, 31], which has recently been developed to handle large boson numbers.

As seen in Figure 2, certain lines representing degeneracies of pairs of levels $[(6_1, 0_2^+), (10_1, 0_3^+), (14_1, 0_4^+)]$ approach the critical region as the boson number

Approximate Symmetries in Nuclear Structure

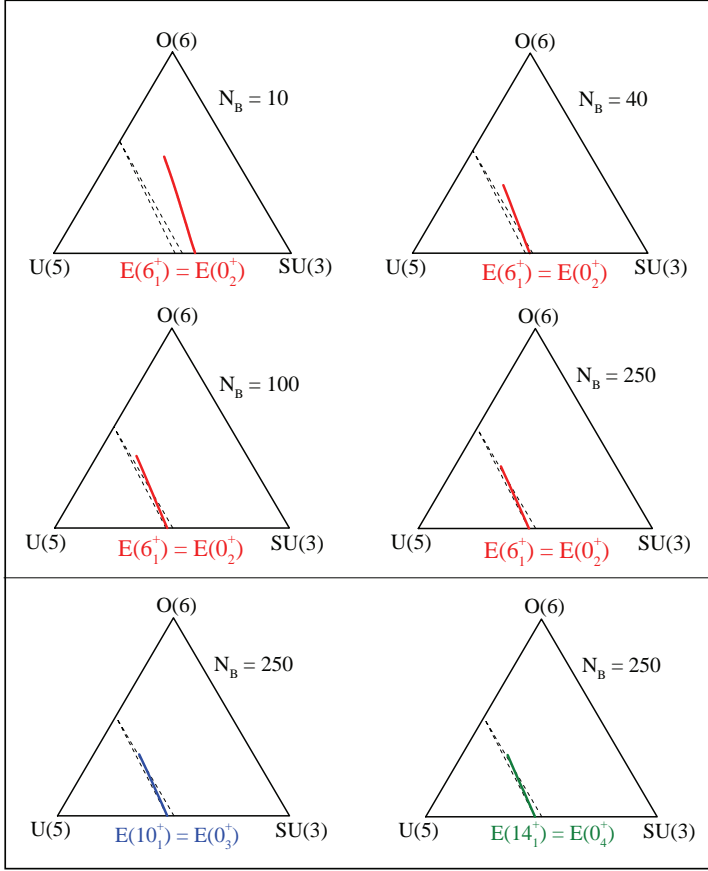


Figure 2. (Top) Line of degeneracy between the 0_2^+ and 6_1^+ levels (solid line) for $N_B = 10, 40, 100,$ and 250 in the IBA triangle. (Bottom) Line of degeneracy between the 0_3^+ and 10_1^+ levels (solid line) for $N_B = 250$ (left) and between the 0_4^+ and 14_1^+ levels (solid line) for $N_B = 250$ (right) in the IBA triangle. The dashed lines denote the critical region in the IBA obtained in the large N_B limit from the intrinsic state formalism [15, 32, 33]. Taken from Ref. [14].

is increased. In Figure 3 one can see that these are degeneracies between members of the ground state band (gsb) and the 0^+ states mentioned in Section 2.

As shown in Table 2, one can see empirically that these states approximately satisfy the expression [13]

$$J(J + 2) = 12n(n + 3), \quad (3)$$

where J indicates the angular momentum of the gsb members, while n enumerates the 0^+ states. These degeneracies maybe indicate the existence of some underlying symmetry, which is yet unknown. Locating this symmetry could

Table 2. Predictions of the IBA (with $N_B = 250$, $\chi = -\sqrt{7}/2$, $\zeta = 0.473$) compared to analytic expressions (see text). On the left, excited 0^+ energies are compared while on the right, energies in the ground state band are compared. Results are normalized to $E(2_1^+) = 1.0$, the numerical factors accompanying $n(n+3)$ and $J(J+2)$ in the column headings reflecting this normalization. Taken from Ref. [13].

n	Analytic $\frac{3}{2}n(n+3)$	IBA $E(0_m^+)$	J	Analytic $\frac{1}{8}J(J+2)$	IBA $E(J)$
1	6.00	6.08	2	1.00	1.00
			4	3.00	3.05
			6	6.00	6.08
			8	10.00	10.00
2	15.00	14.85	10	15.00	14.73
			12	21.00	20.23
3	27.00	27.57	14	28.00	26.43
			16	36.00	33.30
4	42.00	42.55	18	45.00	40.81

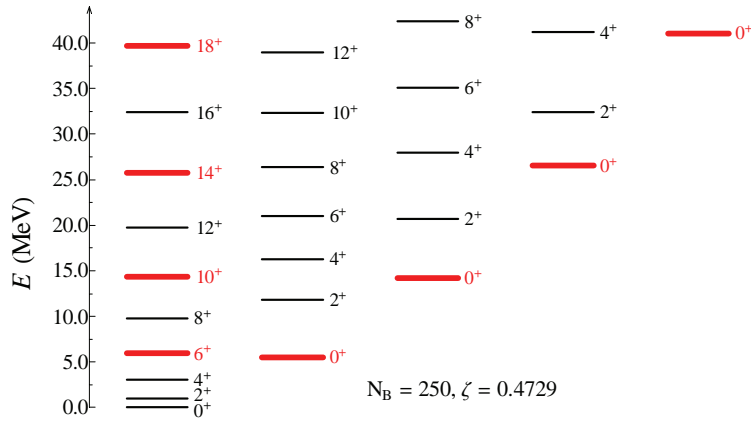


Figure 3. Energies of low-lying states (normalized to $E(2_1^+)=1$) of the Hamiltonian of Eq. (1) with $\chi=-\sqrt{7}/2$, $\zeta=0.4729$, and $N_B=250$. The parameter ζ was chosen to reproduce the approximate degeneracy of $E(0_2^+)$ and $E(6_1^+)$. Taken from Ref. [14].

help in clarifying the nature of the X(5) critical point symmetry, which remains unknown to date.

4 A Quasi-Dynamical Symmetry underlying the Alhassid–Whelan arc of regularity

A puzzle which has been around for nearly 20 years is the existence of the Alhassid–Whelan arc of regularity [19, 20], a region of increased regularity

Approximate Symmetries in Nuclear Structure

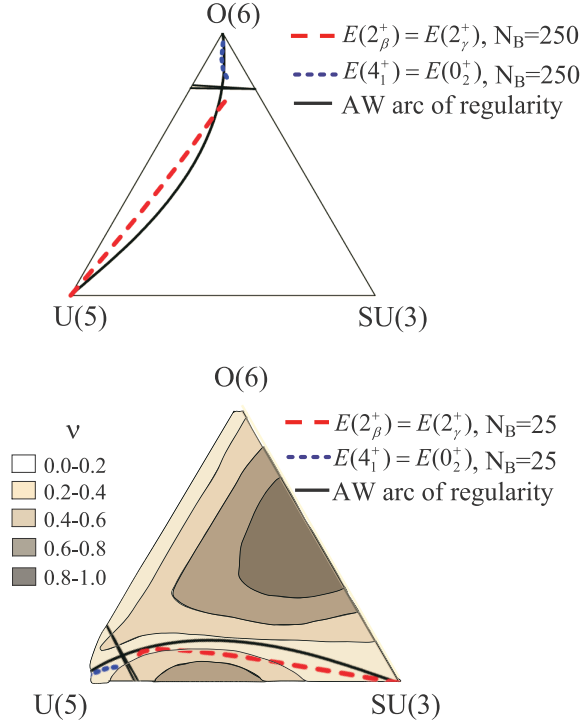


Figure 4. IBA symmetry triangle in the parametrization of Eq. (4) with the three dynamical symmetries and the Alhassid–Whelan arc of regularity. The shape coexistence region [16] between spherical and deformed phases, shown by slanted lines near the U(5) vertex, encloses a first order phase transition terminating in a point of second order transition on the U(5)-O(6) leg. The loci of the degeneracies $E(2_\beta^+) = E(2_\gamma^+)$ (dashed line on the right, corresponding to the QDS discussed in this section) and $E(4_1^+) = E(0_2^+)$ (dotted line on the left) are shown for $N_B=250$ (top) and $N_B = 25$ (bottom). In the bottom part, the ν -diagram, based on Ref. [20] is shown. Taken from Ref. [18].

within the symmetry triangle of the IBM, amidst chaotic regions, as shown in Figure 4. In these studies a different parametrization (using the parameters η, χ) of the IBM Hamiltonian of Eq. (2) has been used, reading [19, 20]

$$H(\eta, \chi) = c \left[\eta \hat{n}_d + \frac{\eta - 1}{N_B} \hat{Q}^x \cdot \hat{Q}^x \right], \quad (4)$$

where the symbols have the same meaning as in Eq. (2).

We shall show that an underlying SU(3) QDS is responsible for the existence of the arc. In order to do so, we shall use some measures of SU(3), like the

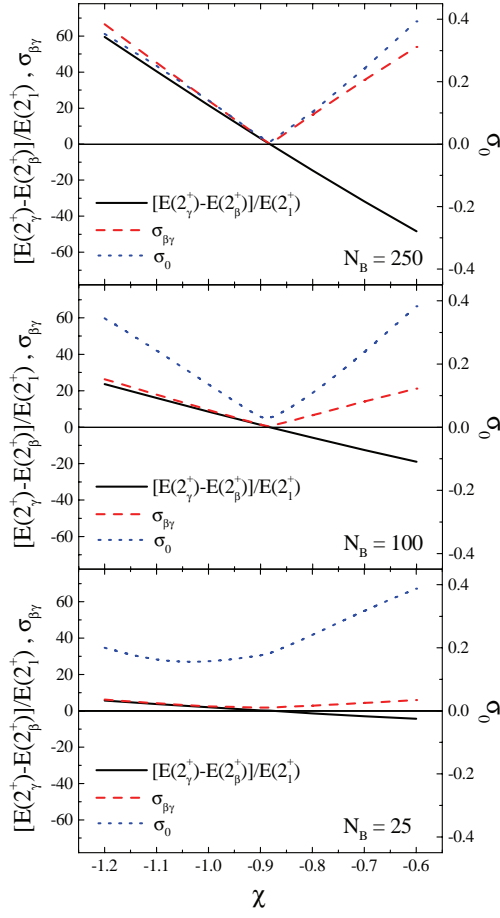


Figure 5. The energy difference $E(2_\gamma^+) - E(2_\beta^+)$ (normalized to $E(2_1^+)$) and the quality measures $\sigma_{\beta\gamma}$ [Eq. (5), up to $L_{\max}=10$] and σ_0 [Eq. (6), up to $i_{\max}=9$], are shown for $\eta=0.632$, varying χ , and boson numbers $N_B=25, 100, 250$. Taken from Ref. [18].

amount of the degeneracy breaking between the β_1 and γ_1 bands [18]

$$\sigma_{\beta\gamma} = \sqrt{\frac{\sum_2^{L_{\max}} [E(L_\beta^+) - E(L_\gamma^+)]^2}{\frac{L_{\max}}{2} - 1}}, \quad (5)$$

where $L_\beta^+ = L_\gamma^+$ and all energies are normalized to $E(2_1^+)$. In order to examine to which degree the 0^+ states occurring in an IBM calculation obey the SU(3) rules, we shall also use the relevant rms deviation of the 0^+ states from the positions

predicted by the second order Casimir operator of SU(3) [18],

$$\sigma_0 = \sqrt{\frac{\sum_3^{i_{\max}} [E(0_i^+)_{th} - E(0_i^+)_{SU(3)}]^2}{i_{\max} - 3}}. \quad (6)$$

with all energies normalized to $E(0_2^+)$ and considering the lowest nine 0^+ states (i.e., $i_{\max}=9$).

As depicted in Figure 5, one can see numerically that both measures of SU(3) behaviour exhibit at large boson numbers strong minima at the point where the degeneracy $2_\gamma^+ = 2_\beta^+$ occurs. This indicates that the spectra acquire an SU(3) structure if this degeneracy is imposed. In Figure 6 one can see that the SU(3) degeneracies appear also at higher bands, well beyond the gsb.

The track of this degeneracy within the symmetry triangle of the IBM shown in Figure 4, nearly coincides with the Alhassid–Whelan arc of regularity, suggesting an underlying SU(3) symmetry as the reason behind the existence of the branch of the arc between the SU(3) vertex and the critical line. In Figure 7 one can see that the SU(3) measures remain close to their SU(3) values far beyond the SU(3) point, thus providing an example of a SU(3) QDS. A similar line, based on the degeneracy $E(4_1^+) = E(0_2^+)$, can be obtained between the U(5) vertex and the critical line, but the relevant minima there are rather shallow, in sharp contrast with the deep minima of Figure 5.

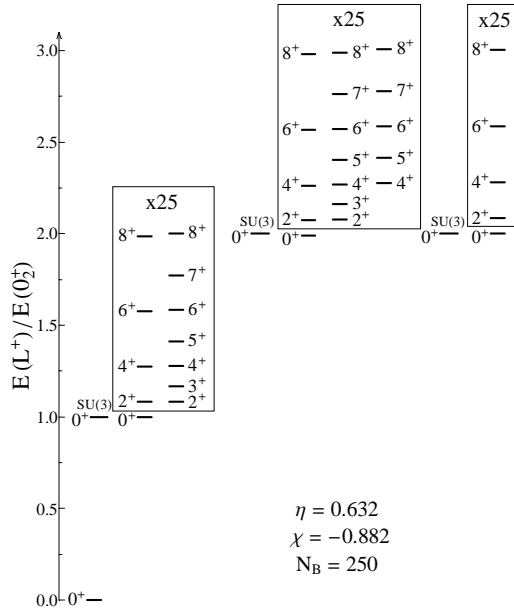


Figure 6. Level scheme for an IBA calculation at a point where $E(2_\beta^+) = E(2_\gamma^+)$. An expanded energy scale (x25) is used within the boxes to show the small rotational energies. The SU(3) 0^+ bandheads are also shown. Taken from Ref. [14].

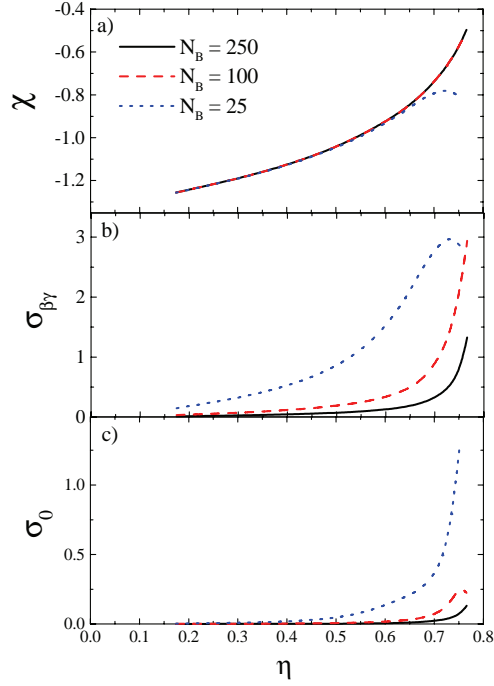


Figure 7. The $|\chi|$ parameter values providing the degeneracy $E(2_{\beta}^{+})=E(2_{\gamma}^{+})$ and the quality measures $\sigma_{\beta\gamma}$ [Eq. (5), up to $L_{\max}=10$] and σ_0 [Eq. (6), up to $i_{\max}=9$], are shown for different values of η and $N_B=25, 100, 250$. Taken from Ref. [14].

5 Conclusion

We have shown some examples of PDS and QDS appearing within special solutions of the Bohr Hamiltonian, as well as in the framework of the IBM. Further searches for approximate symmetries in nuclear structure models appear to be promising.

References

- [1] F. Iachello and A. Arima, *The Interacting Boson Model*, Cambridge University Press, Cambridge (1987).
- [2] R. F. Casten, *Nuclear Structure from a Simple Perspective*, Oxford University Press, Oxford (1990).
- [3] Y. Alhassid and A. Leviatan, *J. Phys. A: Math. Gen.* **25** (1992) L1265.
- [4] A. Leviatan, *Phys. Rev. Lett.* **77** (1996) 818.
- [5] A. Leviatan and P. Van Isacker, *Phys. Rev. Lett.* **89** (2002) 222501.
- [6] A. Leviatan, *Phys. Rev. Lett.* **98** (2007) 242502.
- [7] D. J. Rowe, *Phys. Rev. Lett.* **93** (2004) 122502.

Approximate Symmetries in Nuclear Structure

- [8] D. J. Rowe, P. S. Turner, and G. Rosensteel, *Phys. Rev. Lett.* **93** (2004) 232502.
- [9] D. J. Rowe, *Nucl. Phys. A* **745** (2004) 47.
- [10] P. S. Turner and D. J. Rowe, *Nucl. Phys. A* **756** (2005) 333.
- [11] G. Rosensteel and D. J. Rowe, *Nucl. Phys. A* **759** (2005) 92.
- [12] D. Bonatsos, E.A. McCutchan, and R.F. Casten, *Phys. Rev. Lett.* **101** (2008) 022501.
- [13] D. Bonatsos, E.A. McCutchan, R.F. Casten, R.J. Casperson, V. Werner, and E. Williams, *Phys. Rev. C* **80** (2009) 034311.
- [14] D. Bonatsos, E.A. McCutchan, R.F. Casten, and R.J. Casperson, *Phys. Rev. Lett.* **100** (2008) 142501.
- [15] D.H. Feng, R. Gilmore, and S.R. Deans, *Phys. Rev. C* **23** (1981) 1254.
- [16] F. Iachello, N. V. Zamfir, and R. F. Casten, *Phys. Rev. Lett.* **81** (1998) 1191.
- [17] E. A. McCutchan, D. Bonatsos, and N. V. Zamfir, *Phys. Rev. C* **74** (2006) 034306.
- [18] D. Bonatsos, E. A. McCutchan, and R. F. Casten, *Phys. Rev. Lett.* **104** (2010) 022502.
- [19] Y. Alhassid and N. Whelan, *Phys. Rev. Lett.* **67** (1991) 816.
- [20] N. Whelan and Y. Alhassid, *Nucl. Phys. A* **556** (1993) 42.
- [21] F. Iachello, N.V. Zamfir, and R.F. Casten, *Phys. Rev. Lett.* **81** (1999) 1191.
- [22] R.F. Casten, Dimitri Kusnezov, and N.V. Zamfir, *Phys. Rev. Lett.* **82** (1999) 5000.
- [23] F. Iachello, *Phys. Rev. Lett.* **85** (2000) 3580.
- [24] F. Iachello, *Phys. Rev. Lett.* **87** (2001) 052502.
- [25] D. Bonatsos, D. Lenis, D. Petrellis, P. A. Terziev, and I. Yigitoglu, *Phys. Lett. B* **632** (2006) 238.
- [26] D. Bonatsos, D. Lenis, D. Petrellis, and P. A. Terziev, *Phys. Lett. B* **588** (2004) 172.
- [27] D. Bonatsos, D. Lenis, D. Petrellis, P. A. Terziev, and I. Yigitoglu, *Phys. Lett. B* **621** (2005) 102.
- [28] A. Bohr and B. R. Mottelson, *Nuclear Structure, Vol. II: Nuclear Deformations*, Benjamin, New York (1975).
- [29] V. Werner, N. Pietralla, P. von Brentano, R. F. Casten, and R.V. Jolos, *Phys. Rev. C* **61** (2000) 021301(R).
- [30] R. J. Casperson, Ph.D. thesis, Yale University (2010).
- [31] E. Williams, R.J. Casperson, and V. Werner, *Phys. Rev. C* **77** (2008) 061302(R).
- [32] J.N. Ginocchio and M.W. Kirson, *Phys. Rev. Lett.* **44** (1980) 1744.
- [33] A.E.L. Dieperink, O. Scholten, and F. Iachello, *Phys. Rev. Lett.* **44** (1980) 1747.